# Self-organized noise resistance of oscillatory neural networks with spike timing-dependent plasticity

Oleksandr V. Popovych[1], Serhiy Yanchuk[2], and Peter A. Tass[1,3,4]
[1] *Institute of Neuroscience and Medicine – Neuromodulation (INM-7), Research Center Jülich, 52425 Jülich, Germany*
[2] *Institute of Mathematics, Humboldt University of Berlin, 10099 Berlin, Germany*
[3] *Department of Neuromodulation, University of Cologne, 50924 Cologne, Germany*
[4] *Clinic for Stereotactic and Functional Neurosurgery, University of Cologne, 50924 Cologne, Germany*

# Supplementary Sections

## S1. HODGKIN-HUXLEY NEURAL NETWORK WITH STDP

### A. STDP-induced multistability

The considered Hodgkin-Huxley (HH) ensemble and phase oscillators equipped with the spike timing-dependent plasticity (STDP) demonstrate multistability of limiting states which are characterized by different coupling topologies and collective dynamics. We illustrate such a multistability for the HH network in Fig. S1. For strong enough initial coupling the ensemble converges to a strongly coupled regime where the mean coupling saturates at $\overline{K} \approx 0.25$ [Fig. S1(a), magenta crosses and red circles]. The established strong coupling leads to a strong synchronization which is characterized by large-amplitude oscillations of the population mean field (local field potential) $LFP = N^{-1}\sum_{i=1}^{N} s_i$ [Fig. S1(e), red curve]. If the initial coupling is weak, the ensemble converges to a weakly coupled regime [Fig. S1(a), green triangles and blue diamonds], where the neurons are not synchronized, and the $LFP$ is of low amplitude [Fig. S1(e), green curve]. The extent of synchronization in the neural ensemble can also be evaluated by the order parameter $0 \leq R \leq 1$ [1], where its large values close to 1 are indicative for in-phase synchronization of the neurons firing nearly simultaneously [Fig. S1(f), red dots], whereas small values of $R$ suggest its absence. For the above strongly coupled synchronized and weakly coupled desynchronized regimes the time-averaged order parameters are found $\langle R \rangle \approx 0.92$ and $\langle R \rangle \approx 0.28$, respectively.

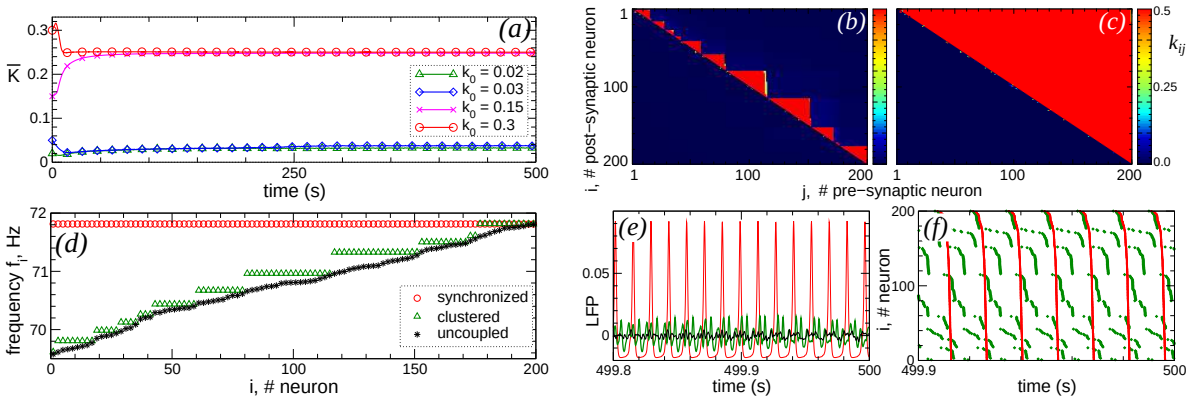


Figure S1: **Plasticity-induced multistability in the HH neural ensemble without input.** (a) Time courses of the mean synaptic weight $\overline{K}(t)$ for different initial coupling matrices $\mathbf{K}(0) = \{k_{ij}(0)\}$, where the coefficients $k_{ij}(0)$ are Gaussian distributed around the mean value $k_0$ as indicated in the legend with standard deviation 0.02. (b), (c) Coupling matrices established in the ensemble due to STDP in the weakly and strongly coupled regimes for $k_0 = 0.02$ and $k_0 = 0.3$, respectively. The matrix elements are encoded in color ranging from 0.0 (blue) to 0.5 (red). For illustration, the neurons are sorted with respect to the increasing natural spiking frequencies $f_i$ such that $f_i \leq f_j$ for $i < j$. (d) Mean spiking frequencies of the neurons in the strongly coupled and synchronized regime (○, corresponding to $k_0 = 0.3$ in (a) and coupling matrix in (c)), weakly coupled and desynchronized regime (△, corresponding to $k_0 = 0.02$ in (a) and coupling matrix in (b)), and uncoupled regime for $k_{ij} \equiv 0$ (∗, natural frequencies). (e) DC-balanced $LFP$ for the strongly coupled regime (red curve) and for the weakly coupled regime (green curve). For comparison, the $LFP$ of the uncoupled ensemble for $k_{ij} \equiv 0$ is depicted by black curve. (f) Raster plot of the firing times in the strongly coupled regime (red dots) and weakly coupled regime (green dots).

In the weakly coupled regime [Fig. S1(b)] several frequency clusters can be formed, where the neurons within the same cluster spike at the same frequency [Fig. S1(d), green triangles] being the natural frequency of the fastest oscillator within the given cluster. Such a clustered dynamics is supported by the established structure of the coupling matrix, where the neurons within the same cluster get strongly coupled to each other [Fig. S1(b)]. Interestingly, the coupling among neurons clearly demonstrates a hierarchical topology, where a fast neuron with larger natural frequency drives slow neurons with smaller natural frequencies, but the coupling in opposite direction vanishes. This holds for both strongly coupled and weakly coupled regimes. For sorted indices of the neurons with respect to increasing their natural spiking frequency, the coupling matrix attains an upper-triangular structure [Fig. S1(b), (c)]. Such a coupling topology is resulted from the asymmetry of the considered STDP rule and phase locking of the neurons to each other, see Refs.[2, 3]. Indeed, if two neurons $i$ and $j$ synchronize, the time difference $\Delta t_{ij} = t_i - t_j$ between the nearest spike onsets $t_i$ and $t_j$ of the post- and pre-synaptic neurons $i$ and $j$, respectively, gets narrowly distributed or even constant [Fig. S1(f), red dots]. Moreover, in the perfect phase-locked regime, a faster neuron spikes before a slower one does, and only synaptic weight from faster neuron to slower one will be potentiated, while the coupling in opposite direction will be depressed.

For illustration, consider a post-synaptic neuron $i = 100$ and two pre-synaptic neurons $j = 50$ and $j = 150$. Because the natural spiking frequency of neuron $i = 100$ is smaller than that of neuron $j = 150$ (the neurons' indices are sorted), in the phase-locked regime the spikes of the pre-synaptic neuron 150 advance the spikes of the post-synaptic neuron 100. We found that the corresponding time difference $\Delta t_{100,150} \approx 0.5$ms [Fig. S2(a), right red vertical line], and the synaptic weight $k_{100,150}$ is potentiated by $\delta \cdot W(0.5) \approx 0.76\delta$ at the moment when neuron $i = 100$ fires. Since the coupling strength $k_{ij}$ is updated when either neuron $i$ or neuron $j$ fires, the synaptic weight $k_{100,150}$ is depressed by $\delta \cdot W(-13.4) \approx -0.05\delta$ at the moment when the pre-synaptic neuron $j = 150$ fires, and $\Delta t_{100,150} \approx -13.4$ ms is the corresponding spike time difference [Fig. S2(a), left red vertical line]. In such a way, synaptic weight $k_{100,150}$ from the

faster neuron $j = 150$ to the slower neuron $i = 100$ will in average be updated by $0.71\delta$, i.e., it is continuously potentiated until it saturates at the maximal admissible value $k_{100,150} = k_{\max}$.

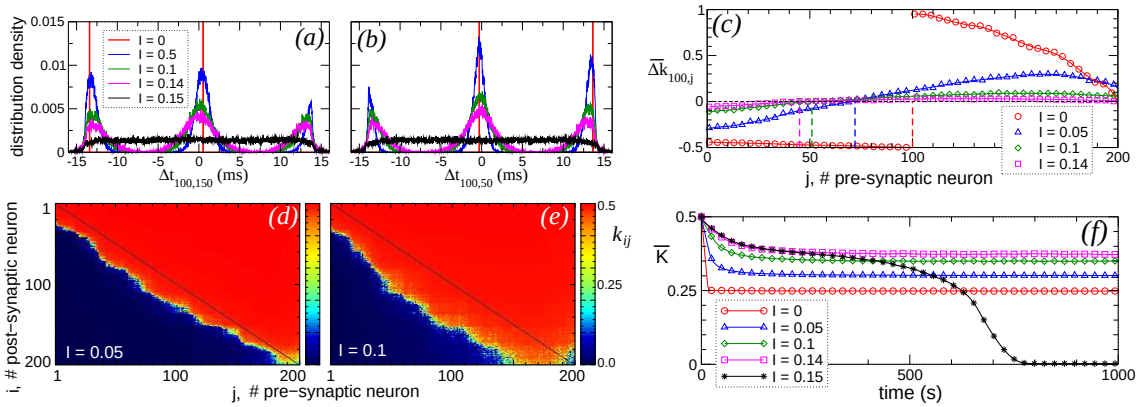


Figure S2: **Noise-induced dynamics of synaptic weights in the HH neural network with STDP.** (a), (b) Distribution densities $\rho_{ij}$ of the spike time differences $\Delta t_{100,150}$ and $\Delta t_{100,50}$, respectively, established for the input intensities $I$ indicated in the legend. (c) Average update rate $\overline{\Delta k}_{100,j}$ of synaptic weights calculated by integrating the plasticity function $W$ over the distribution densities $\rho_{100,j}$ according to equation (S1). Vertical dashed lines of the corresponding colors indicate the index $j$ where $\overline{\Delta k}_{100,j}$ crosses zero. (d) and (e) Coupling matrices established in the neural ensemble for $I = 0.05$ and $I = 0.1$, respectively. (f) Time courses of the mean synaptic weight $\overline{K}$ for different input intensities $I$ indicated in the legend. The initial synaptic weights $k_{ij}(0)$ are Gaussian distributed around the mean value $k_0 = 0.5$ with standard deviation 0.02.

The situation is opposite for synaptic weight $k_{100,50}$ because, in this case, the spikes of the slower pre-synaptic neuron $j = 50$ follow those of the faster post-synaptic neuron $i = 100$. The synaptic weight $k_{100,50}$ is in average updated by $\delta W(13.6) + \delta W(-0.3) \approx -0.48\delta$, where $\Delta t_{100,50} = 13.6$ ms and $\Delta t_{100,50} = -0.3$ ms are the corresponding spike time differences calculated at the moments when neuron $i = 100$ and neuron $j = 50$ fires, respectively [Fig. S2(b), red vertical lines]. Then the coupling from the slower neuron $j = 50$ to the faster neuron $i = 100$ is depressed until it saturates at the minimal admissible value $k_{100,50} = k_{\min}$. In such a way the uni-directional hierarchical coupling topology illustrated in Fig. S1(b) and (c) establishes in the neural network. For the strongly coupled regime, each neuron drives all slower neurons and receives the driving only from the faster neurons. Then the population synchronizes at the frequency of the fastest oscillator [Fig. S1(d), red circles]. The same is true for the weakly coupled regime for each frequency cluster [Fig. S1(d), green triangles].

### B. Noise-induced dynamics

An independent random input broadens the distribution of the spike time differences $\Delta t_{ij}$ [Fig. S2(a),(b)]. Such a change of the relative firing times influences the update of synaptic weights which, in turn, have an impact on the distribution of $\Delta t_{ij}$. In the course of such a self-organization process, limiting distribution densities $\rho_{ij}(\Delta t)$ of the spike time differences $\Delta t_{ij}$ set up [Fig. S2(a), (b)]. Then the average update rate of the synaptic weights can be calculated by the formula (equation (1) in the main text)

$$\overline{\Delta k}_{ij} = \int W(\xi)\rho_{ij}(\xi)d\xi. \tag{S1}$$

For the input-free and strongly coupled regime the distribution densities $\rho_{ij}(\Delta t)$ have a delta-peak shape [Fig. S2(a), (b), red vertical lines], and equation (S1) gives the same values for the average update

rates as calculated above for the synaptic weights $k_{100,150}$ and $k_{100,50}$. Random input induces changes of $\rho_{ij}$ and $\overline{\Delta k}_{ij}$ where the latter becomes positive (synaptic weights $k_{ij}$ will be potentiated) for a bigger range of the neurons' indices. For example, $\overline{\Delta k}_{100,j}$ is positive for $j > 100$ at $I = 0$, $j > 70$ at $I = 0.05$, $j > 50$ at $I = 0.1$, and $j > 44$ at $I = 0.14$ [Fig. S2(c)]. The corresponding synaptic weights $k_{100,j}$ will thus be potentiated for the given input intensity, and the post-synaptic neuron $i = 100$ receives coupling from much more neurons as compared to the noisy-free case. In such a way the coupling matrix will gain positive coefficients below the main diagonal [Fig. S2(d), (e)], and the mean synaptic weight grows as the strength of the random input increases [Fig. S2(f)], see also Fig. 1 of the main text.

For large intensity of the random input the synchronized firing of the neurons is significantly perturbed, in particularly, for fast neurons which get decoupled from the rest of the population. The decoupling then propagates to the interior of the coupling matrix as time evolves such that, in the limit, all neurons get fully decoupled and desynchronized [Fig. S2(f), black asterisks], see also Supplementary Video 1 where the time course of the coupling matrix is animated for the input intensity $I = 0.15$.

### C. Inhibitory random input and Gaussian noise

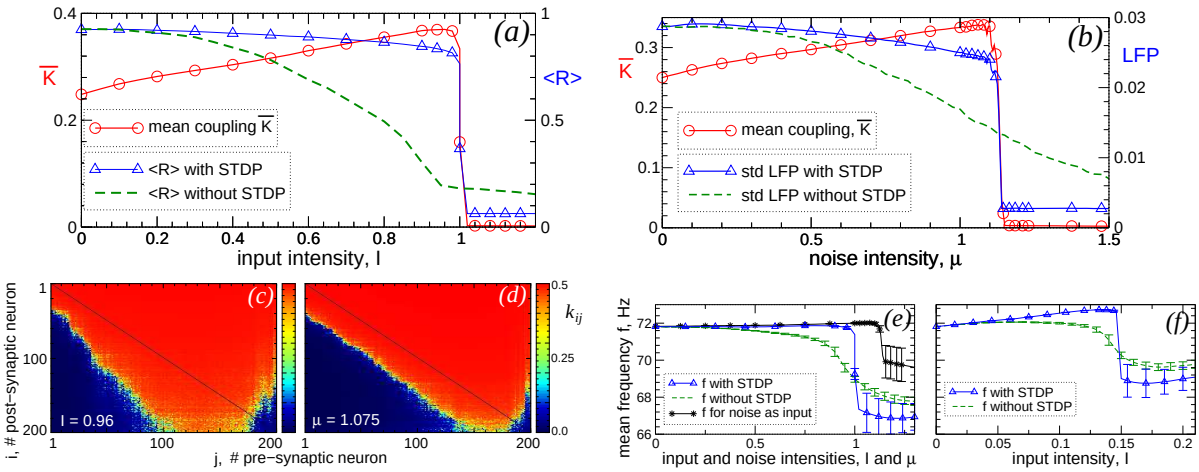


Figure S3: **Constructive effects of the independent random inhibitory input and white noise on the dynamics of synaptic weights of the HH ensemble.** (a), (b) Mean synaptic weights $\overline{K}$ (○—○, scales on the left vertical axes), (a) time-averaged order parameter $\langle R \rangle$ and (b) standard deviation (std) of $LFP$ for the ensemble with STDP (△–△) and without STDP (– –) versus (a) intensity $I$ of independent random inhibitory input and (b) strength $\mu$ of the independent Gaussian noise. For $\langle R \rangle$ and std $LFP$ the scales are given on the right vertical axes. For the network without STDP, the coupling matrix is fixed $\mathbf{K}_{\rm Fix} = \{k_{ij}\}$, $k_{ij} = 0.5$ for $j > i$ and $k_{ij} = 0$ otherwise, as in the strongly coupled regime without perturbations [Fig. S1(c)]. (c), (d) Coupling matrices for the cases of synaptic inhibitory and noise input and for optimal input strength $I = I_{\rm opt} = 0.96$ and $\mu = \mu_{\rm opt} \approx 1.075$, respectively, where $\overline{K}$ is maximal, see plots (a) and (b). (e), (f) Mean frequency $f$ of the HH ensemble for (e) inhibitory synaptic input and (f) excitatory synaptic input for the ensemble with STDP (△–△) and without STDP (– –). In plot (e) the mean frequency of the HH ensemble with STDP is also shown for the noise input (∗—∗). Error bars indicate the standard deviation over the ensemble.

The reported effects induced by the independent random excitatory synaptic input $I_i^{\rm input}(t)$ [Fig. 1 of the main text] are nearly identically preserved if the inter-spike intervals (ISI) of the input post-synaptic potentials (PSP) are independently distributed according to a Poisson distribution with mean and variance $\lambda = 14$ ms (not shown). The same results can be obtained for a Gaussian independent random inhibitory synaptic input by considering the reverse potential $V_r = -50$ mV in equation (6) of the main text. The main difference here is a larger range of the input intensity $I$, where the mean

synaptic weight grows with increasing $I$ [Fig. S3(a), (c)]. For this simulation the update of synaptic weights is taken in the form $k_{ij} \to k_{ij} + \delta \cdot \sum W(\Delta t_{ij})$, and the sum is taken by all spikes of the pre- or post-synaptic neuron fitting between the last two spikes of the firing neuron.

Qualitatively the same conclusions can be drawn for an independent white noise: The HH neurons are subjected to an additive noise $I_i^{\rm input}(t) = \mu\xi_i(t)$, where $\xi_i$ are independent normally distributed random variables, $\langle \xi_i \rangle = 0$ and $\langle \xi_i(t), \xi_j(t') \rangle = \delta(i-j)\delta(t-t')$. Parameter $\mu$ controls the noise intensity. In this case the noise can be considered as a direct somatic stimulation as compared to a synaptically-mediated input, see Ref. [4]. As for synaptic input, the noise induces an increase of the amount of coupling in the HH neural ensemble with STDP, and there exists an optimal noise strength $\mu_{\rm opt}$ where the mean synaptic weight $\overline{K}$ is maximal [Fig. S3(b)]. Also the coupling matrix attains a similar structure, and the noise leads to the emergence of connections from slow to fast neurons [Fig. S3(d)]. STDP significantly counteracts the suppression of synchronization in the neural ensemble by the noise as reflected by the behavior of the $LFP$ [Fig. S3(b)]. For example, the standard deviation (std) of $LFP \approx 0.024$mV for the noise of intensity $\mu = 1.1$ in the ensemble with STDP [Fig. S3(b), blue triangles], whereas std $LFP \approx 0.014$mV for the same noise strength in the ensemble without STDP and fixed coupling matrix $\mathbf{K}_{\rm Fix}$ [Fig. S3(b), green dashed curve]. This corresponds to 16% and 51% of the relative suppression of synchronization, respectively, as related to the noisy-free case where std $LFP \approx 0.0287$mV.

The random input does not significantly influence the frequency of synchronized neurons with STDP, as illustrated in Fig. S3 (e) and (f). Only the excitatory synaptic input may slightly accelerate the oscillations from 71.8 Hz to 72.7 Hz [Fig. S3 (f), blue triangles], whereas the noise input keeps the mean frequency nearly constant, and the inhibitory input slightly slows the neurons down [Fig. S3 (e), black asterisks and blue triangles].

## S2. PHASE OSCILLATORS

### A. Noise-free phase differences

We derive expression (2) of the main text for the phase shifts $\varphi_j$ of the locked phase oscillators for the fixed upper-triangular coupling matrix $\mathbf{K}_{\rm Fix} = \{k_{ij}\}$ as in the strongly coupled regime, i.e., $k_{ij} = k = 1$ for $i < j$, and $k_{ij} = 0$ otherwise. For this we consider the ensemble of locked phases $\psi_i = \omega t + \varphi_i$, where the synchronization frequency $\omega = \omega_N$ is the largest natural frequency of the phase-locked oscillators for such a coupling topology, see Fig. S1(d). The equations then read

$$\dot{\varphi}_i = \tilde{\omega}_i + \frac{k}{N} \sum_{j>i} (\sin\varphi_j \cos\varphi_i - \cos\varphi_j \sin\varphi_i), \tag{S2}$$

where $\tilde{\omega}_i = \omega_i - \omega_N$, $i = 1, 2, \ldots, N$. Since the phase shifts $\varphi_i$ are constant in the phase-locked regime, we obtain

$$C_{i+1} \sin\varphi_i - S_{i+1} \cos\varphi_i = \frac{N\tilde{\omega}_i}{k}, \tag{S3}$$

where $S_{i+1} = \sum_{j=i+1}^{N} \sin(\varphi_j)$ and $C_{i+1} = \sum_{j=i+1}^{N} \cos(\varphi_j)$. Denoting $D_{i+1} = S_{i+1}^2 + C_{i+1}^2$ and dividing equation (S3) by $\sqrt{D_{i+1}}$ we arrive to

$$\sin(\varphi_i - \theta_{i+1}) = \frac{N\tilde{\omega}_i}{k\sqrt{D_{i+1}}}, \tag{S4}$$

where $\sin(\theta_{i+1}) = S_{i+1}/\sqrt{D_{i+1}}$ and $\cos(\theta_{i+1}) = C_{i+1}/\sqrt{D_{i+1}}$. From the last equation we obtain expression (2) of the main text

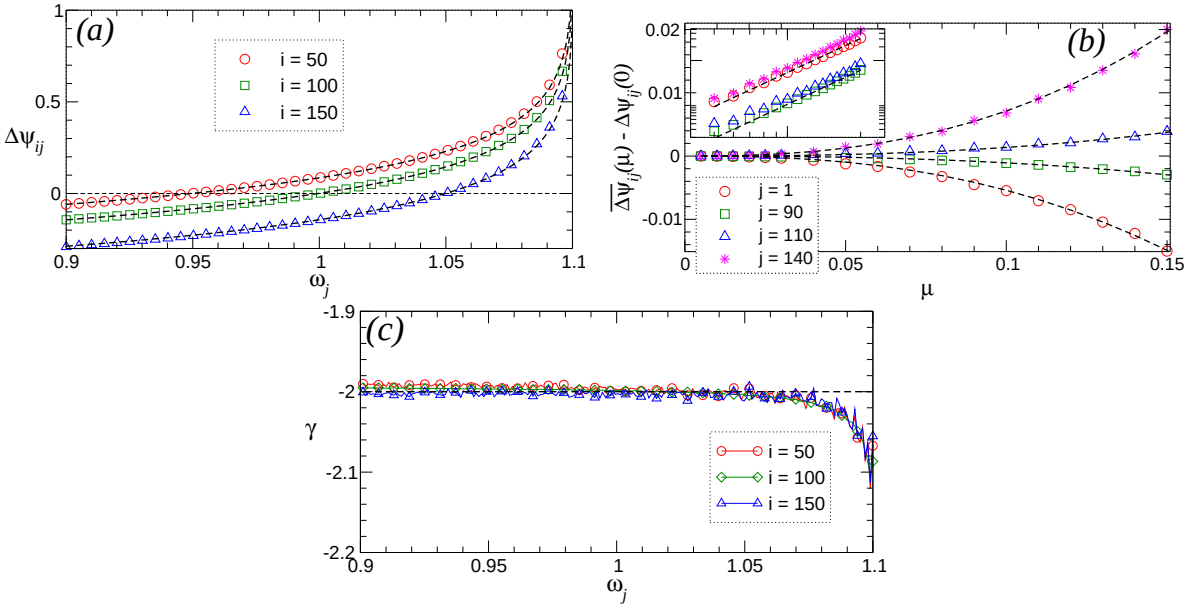


Figure S4: **Noise-induced distribution of the phase differences for fixed coupling matrix $\mathbf{K}_{\mathrm{Fix}}$.** (a) Phase differences $\Delta\psi_{ij}$ versus the natural frequency $\omega_j$ of the pre-synaptic oscillator $j$ for fixed post-synaptic oscillators $i$ as indicated in the plot. The dashed black curves depict the theoretical prediction from equation (S5), and symbols illustrate the mean (time-averaged) phase differences $\overline{\Delta\psi}_{ij}(\mu)$ obtained from numerical simulations for the noise intensity $\mu = 0.05$. (b) Deviations of the mean phase differences $\overline{\Delta\psi}_{ij}(\mu)$ from the noise-free phase differences $\Delta\psi_{ij}(0)$ versus noise intensity for $i = 100$ and indices $j$ indicated in the legend. The dashed black curves depict the function $a \cdot \mu^{2.5}$ for fitted values of coefficient $a$. In the subplot the absolute values of the deviations are shown in log-log scale. (c) Numerically fitted exponent $\gamma$ of the concentration parameter $\kappa(\Delta\psi_{ij}) \sim \mu^{\gamma}$ versus natural frequency of the pre-synaptic oscillators for three fixed post-synaptic oscillators $i$ as indicated in the legend. The natural frequencies $\omega_i$ are uniformly distributed in the interval $[0.9,\, 1.1]$, $\omega_i = 0.9 + 0.2(i-1)/(N-1)$.

$$\varphi_i = \arcsin\left(\frac{S_{i+1}}{\sqrt{D_{i+1}}}\right) + \arcsin\left(\frac{N\tilde{\omega}_i}{k\sqrt{D_{i+1}}}\right), \tag{S5}$$

and can calculate the phase differences $\Delta\psi_{ij} = \psi_j - \psi_i = \varphi_j - \varphi_i$ by letting $\varphi_N = 0$ [Fig. S4(a), black dashed curves].

### B. Noise-induced distribution of phase differences

We found that the mean (averaged over time) phase differences $\overline{\Delta\psi}_{ij}$ are only slightly influenced by a weak noise, see Fig. S4(a). However, if the noise increases, the mean phase differences $\overline{\Delta\psi}_{ij}$ start to deviate from those of the noise-free phase ensemble according to a power law $\sim \mu^{\lambda}$ with $\lambda \approx 2.5$ which seems to be independent of the natural frequencies of the oscillators [Fig. S4(b)]. For a complete description of the noise-induced dynamics of the phase differences, the above behavior of $\overline{\Delta\psi}_{ij}$ has to be taken into account. In this study we neglect it, since we are interested in the effect of weak to moderate noise.

We approximate the noise-induced distribution of the phase differences $\Delta\psi_{ij}$ of the phase ensemble with fixed coupling matrix $\mathbf{K}_{\mathrm{Fix}}$ by the von Mises distribution (equation (3) of the main text)

$$M(\kappa, \varphi) = \frac{1}{2\pi I_0(\kappa)} \exp(\kappa \cos(\varphi - \varphi_0)), \tag{S6}$$

and find the concentration parameters $\kappa$ and mean phase differences when noise intensity varies. For small values of $\kappa$, the von Mises distribution is close to a uniform distribution, whereas for large values of $\kappa$ it approaches a Gaussian distribution with mean $\varphi_0$ and variance $1/\kappa$ [5]. The von Mises distribution (S6) can thus be used to approximate the spectrum of possible spreads of the phase differences $\Delta\psi_{ij}$ of well synchronized noisy oscillators with narrowly distributed phase differences as well as of desynchronized oscillators where the their phase differences fill the entire unit circle with a nearly uniform distribution. We found that the considered von Mises distribution (S6) well approximates the statistics of the noisy phase differences for the corresponding parameters $\kappa$ and $\varphi_0$, see Fig. 3(a) of the main text.

Interestingly, parameter $\kappa$ fitted to the distribution of the phase differences obtained by numerical simulations demonstrates a power-law dependence on the noise strength $\kappa(\Delta\psi_{ij}) \sim \mu^{\gamma}$, see Fig. 3(b) of the main text. Moreover, the exponent $\gamma$ seems to be independent of the natural frequencies of the oscillators $i$ and $j$. We plot $\gamma$ versus the natural frequency $\omega_j$ of the pre-synaptic oscillators for different post-synaptic oscillators $i$ in Fig. S4(c). As one can see, $\gamma \approx -2$ except for fast oscillators with large $\omega_j$. The fast oscillators of the ensemble are sensitive to noise and may get desynchronized by noise with the other oscillators with broadly distributed phase differences, see Fig. 3(a) of the main text for $j = 200$. Then, for a large noise, the behavior of the concentration parameter $\kappa(\Delta\psi_{ij})$ may slightly deviate from the above power law for large natural frequencies, and the fitted parameter $\gamma$ somewhat departs from the value $-2$ for large $\omega_j$ [Fig. S4(c)] . However, the above power law with $\gamma = -2$ is satisfied either for small noise or for not particularly large natural frequencies, and we use it for our theoretical approximation.

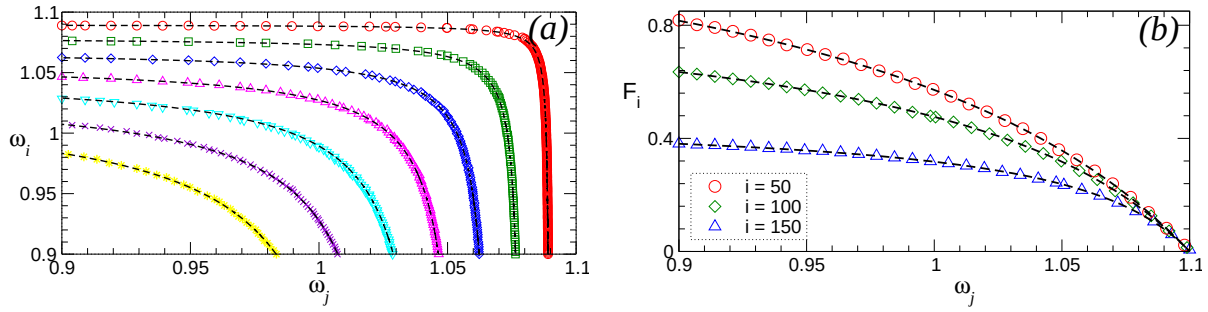


Figure S5: **Approximation of the frequency dependence of the concentration parameter $\kappa$.** (a) Contour lines of the function $F(\omega_i, \omega_j) \equiv F_{const}$ for the values $F_{const} = 0.1$ (○), 0.2 (□), 0.3 (◇), 0.4 (△), 0.5 (▽), 0.6 (×), and 0.7 (✳). The black dashed curves depict the fitting by the formula (S7) with parameters in Table S1. (b) Function $F_i(\omega_j) = F(\omega_i, \omega_j)$ for three post-synaptic oscillators $i$ as indicated in the legend. The dashed black curves show the theoretical approximation of $F(\omega_i, \omega_j)$ for $\beta = -9.52$, while symbols illustrate the results of numerical simulations for noise $\mu = 0.1$. Other parameters as in Fig. S4.

### C. Frequency dependence of the concentration parameter $\kappa$

Below we show how we obtained the form of function $F(\omega_i, \omega_j) = \beta\tilde{\omega}_i\tilde{\omega}_j/(\tilde{\omega}_i + \tilde{\omega}_j)$ in expression (4) of the main text for the concentration parameter $\kappa$ of the von Mises distribution. For this we fix the noise strength, e.g., $\mu = 0.05$ and calculate $\kappa(\Delta\psi_{ij})$ by numerical fitting of the phase difference distribution densities by the von Mises distribution for different indices $i$ and $j$, i.e., for different natural frequencies $\omega_i$ and $\omega_j$. Since the exponent $\gamma$ in equation (4) of the main text seems to be independent of the natural frequencies [Fig. S4(c)], we calculate $F(\omega_i, \omega_j) = \kappa(\Delta\psi_{ij})/\mu^{\gamma}$ with $\gamma = -2$. The contour lines $F(\omega_i, \omega_j) \equiv F_{const}$ in the parameter plane $(\omega_i, \omega_j)$ are shown in Fig. S5(a) for different values of $F_{const}$. We found that the contour lines align along symmetric hyperbolas

$$(\omega_i - B)(\omega_j - B) = A, \tag{S7}$$

| $F_{const}$ | 0.1 | 0.2 | 0.3 | 0.4 | 0.5 | 0.6 | 0.7 |
|---|---|---|---|---|---|---|---|
| $A$ | 0.000124 | 0.000459 | 0.000994 | 0.001755 | 0.002838 | 0.003854 | 0.005548 |
| $B$ | 1.0897 | 1.0790 | 1.0682 | 1.0576 | 1.0478 | 1.0357 | 1.0270 |
| $Res$ | 0.000017 | 0.000018 | −0.000017 | −0.000043 | 0.00011 | −0.00028 | 0.00022 |
| $B_0$ | −0.103 | −0.105 | −0.106 | −0.106 | −0.104 | −0.107 | −0.104 |

Table S1: Parameters of the numerical fitting of function $F(\omega_i, \omega_j)$.

where parameters $A$ and $B$ can be found by numerical fitting of the contour lines and are listed in Table S1. We represent parameter $B = B_0 F_{const} + \omega_N$ and rewrite equation (S7) in the form

$$(\omega_i - \omega_N)(\omega_j - \omega_N) - B_0 F_{const} \left[(\omega_i - \omega_N) + (\omega_j - \omega_N)\right] = A - B_0^2 F_{const}^2. \tag{S8}$$

Interestingly, the residual term $Res = A - B_0^2 F_{const}^2$ attains very small values, while $B_0$ slightly fluctuates around $\overline{B}_0 = -0.105$, see Table S1. We thus neglect the term $A - B_0^2 F_{const}^2$ and set $B_0 = -0.105$ in equation (S8), which leads to the above form of function $F(\omega_i, \omega_j)$ with parameter $\beta = 1/B_0 \approx -9.52$. Finally, we verified the obtained empirical formula of $F(\omega_i, \omega_j)$ for other values $\mu$ of the noise strength and found a perfect agreement with numerical simulations, see Fig. S5(b).

## S3. SUPPLEMENTARY VIDEOS

**Video 1:** Animated time course of the coupling matrix of the HH neural ensemble with STDP and independent random synaptic excitatory input of intensity $I = 0.15$. The synaptic weights $k_{ij}$ are encoded in color ranging from 0 (blue) to 0.5 (red). The elements of the initial coupling matrix $\mathbf{K}(0) = \{k_{ij}(0)\}$ are Gaussian distributed around the mean value $\overline{K}(0) = 0.5$ with standard deviation 0.02. The STDP and input are switched on at time $t = 100$ s.

**Video 2:** Animated time course of the coupling matrix of the phase ensemble with STDP and independent Gaussian noise of intensity $\mu = 0.185$. The coupling weights $k_{ij}$ are encoded in color ranging from 0 (blue) to 1 (red). The elements of the initial coupling matrix $\mathbf{K}(0) = \{k_{ij}(0)\}$ are Gaussian distributed around the mean value $\overline{K}(0) = 1$ with standard deviation 0.01. The STDP and noise are switched on at time $t = 2000$ ms. The time was accelerated after $t = 30$ s.


[1] Kuramoto, Y. *Chemical oscillations, waves, and turbulence* (Springer, Berlin Heidelberg New York, 1984).

[2] Masuda, N. & Kori, H. Formation of feedforward networks and frequency synchrony by spike-timing-dependent plasticity. *J. Comput. Neurosci.* **22**, 327–345 (2007).

[3] Bayati, M. & Valizadeh, A. Effect of synaptic plasticity on the structure and dynamics of disordered networks of coupled neurons. *Phys. Rev. E* **86**, 011925 (2012).

[4] Popovych, O. V. & Tass, P. A. Desynchronizing electrical and sensory coordinated reset neuromodulation. *Front. Hum. Neurosci.* **6**, 58 (2012).

[5] Mardia, K. & Jupp, P. *Directional Statistics* (Wiley, Chichester New York, 2009).